Biosensors and Bioelectronics 44 (2013) 77–84

Contents lists available at SciVerse ScienceDirect

Biosensors and Bioelectronics

journal homepage: www.elsevier.com/locate/bios

Integration of gold nanoparticles in PDMS microfluidics for lab-on-a-chip plasmonic biosensing of growth hormones

Hamid SadAbadi [a,b], Simona Badilescu [a], Muthukumaran Packirisamy [a,*], Rolf Wüthrich [b]

[a] Optical-Bio Microsystems Laboratory, Department of Mechanical Engineering, Concordia University, 1515 Saint Catherine Street West, EV13.235, Montreal, Quebec, Canada H3G 1M8

[b] Electrocatalytic Green Engineering Group, Department of Mechanical Engineering, Concordia University 1515 Saint Catherine Street West, EV14.205, Montreal, Quebec, Canada H3G 1M8

ARTICLE INFO

Article history:
Received 21 September 2012
Received in revised form
5 December 2012
Accepted 2 January 2013
Available online 16 January 2013

Keywords:
Nano-microfluidic integrated biosensor
Gold–PDMS nanocomposite
In-situ reduction
Bovine somatotropin (bST)
Localized surface plasmon resonance (LSPR)
Chemical kinetics

ABSTRACT

Gold nanoparticles were synthesized in a poly(dimethylsiloxane) (PDMS) microfluidic chip by using an *in-situ* method, on the basis of reductive properties of the cross-linking agent of PDMS. The proposed integrated device was further used as a sensitive and low-cost LSPR-based biosensor for the detection of polypeptides.

Synthesis of nanoparticles in the microfluidic environment resulted in improvement of size distribution with only 8% variation, compared with the macro-environment that yields about 67% variation in size. The chemical kinetics of the *in-situ* reaction in the microfluidic environment was studied in detail and compared with the reaction carried out at the macro-scale. The effect of temperature and gold precursor concentration on the kinetics of the reaction was investigated and the apparent activation energy was estimated to be $E_a^* = 30$ kJ/mol.

The sensitivity test revealed that the proposed sensor has a high sensitivity of 74 nm/RIU to the surrounding medium. The sensing of bovine growth hormone also known as bovine somatotropin (bST) shows that the proposed biosensor can reach a detection limit of as low as 3.7 ng/ml (185 pM). The results demonstrate the successful integration of microfluidics and nanoparticles which provides a potential alternative for protein detection in clinical diagnostics.

1. Introduction

The development of biosensors for the detection of different biomolecules is an extremely important problem in life science and clinical diagnostics. With the recent advances in optics, microfabrication and nanotechnology, new biosensing methods are emerging for the development of sensitive and low-cost integrated biosensors (Arlett et al., 2011; Haes and Van Duyne, 2002; Zhang et al., 2012).

Bovine somatotropin (bST) is a growth promoter widely used (in some countries) in dairy farming to increase the milk production. It has been reported that the concentration of bST, also known as bovine growth hormone (BGH), in milk could be less than 10 ng/ml (McGrath et al., 2008). Indeed, the concentration of the growth hormone has to be controlled very strictly in milk because of possible health issues (Ozhikandathil and Packirisamy, 2012).

The commercial use of growth hormone was made possible with the discovery of the recombinant bovine somatoropin (rbST) produced using recombinant DNA technology. When rbST is used to increase the milk production in cattle, its traces can be found in the milk of a treated cattle with concentrations in the order of hundreds of ng/ml (Le Breton et al., 2010). However, it has been proved that the administration of rbST rises the concentration of insulin-like growth factor-I (IGF-I). This compound may accumulate in the body of animals as well as consumers and it has a long-term effect with possible consequences on health. Therefore, the need for a sensing method that can monitor the concentration of rbST (and bST) becomes very critical (Ozhikandathil et al., 2012; Ozhikandathil and Packirisamy, 2012).

The development of immunosensors based on plasmonic properties of gold colloids is expanding rapidly in recent times (Barnes et al., 2003). The interest in LSPR-based biosensors relies on their unique properties allowing label-free and real-time biomolecular analysis with possible detection of biomolecular interactions (antigen–antibody interaction, DNA hybridization, etc.) at low concentrations (Haes and Van Duyne, 2004; Hoa et al., 2009). In addition, the simple detection mechanism of optical-based biosensors makes it possible to be integrated with different sensing platforms for lab-on-a-chip

* Correspondence to: Optical-Bio MEMS Laboratory, Deptartment of Mechanical and Industrial Engineering, Concordia University, EV4-149, 1515 Saint Catherine Street West, EV13.235 Montreal, Quebec, Canada H3G 1M8.
Tel.: +1 514 8482424x7973; fax: +1 514 848 3175.
E-mail address: pmuthu@alcor.concordia.ca (M. Packirisamy).
URL: http://www.mie.concordia.ca/mems (M. Packirisamy).

0956-5663/$ - see front matter © 2013 Elsevier B.V. All rights reserved.
http://dx.doi.org/10.1016/j.bios.2013.01.016

applications such as integrated microfluidic devices (Badilescu and Packirisamy, 2012; Cheng et al., 2009; Lin et al., 2010).

Microfluidics based biosensing is of interest for a wide spectrum of scientists from physicists and chemists to biologists due to their high-throughput and low-cost mass fabrication (Ben-Yoav et al., 2012). The combination of microfluidic devices with LSPR biosensors offers some significant advantages from both technologies and results in an improvement of overall performance of the biosensor. Indeed, a microfluidic device reduces significantly the required sample/reagent volume. In addition, miniaturized channel footprints may result in an accelerated immunoreaction and fast response (Luo et al., 2008).

Several papers on the integration of nanoparticles into the microfluidic devices for biosensing application have been published recently (Abbas et al., 2011; Zhang et al., 2012). However, in the majority of these works, pre-synthesized NPs were introduced into the microfluidic system (Hsu et al., 2011; Huang et al., 2009a, 2009b; Li et al., 2005; Qiu et al., 2009; Trung et al., 2012). In addition, physical methods were also used to fabricate nanoparticles inside a microfluidic chip such as soft-lithography (Haes and Van Duyne, 2002) and physical vapor deposition (Geng et al., 2011). There are very few works that use *in-situ* methods for the synthesis of nanostructures (Kim et al., 2012) and nanoparticles (Trung et al., 2012; Zhou et al., 2010) inside a microchannel for different bio-applications.

For biosensing experiments in a polydimethylsiloxane (PDMS) microfluidic device, gold nanoparticles (AuNPs) need to be immobilized very well on the surface of the channel. By using an *in-situ* synthesis method, gold nanoparticles crystalize and grow inside the polymer network during the reaction. To the best of our knowledge, the proposed *in-situ* technique would ensure high stability of the gold nanoparticles in the channel. In this way, the AuNPs are embedded in the polymer to interact strongly with the polymer network (SadAbadi et al., 2012).

As we mentioned earlier, in order to integrate gold nanoparticles into a PDMS microfluidics, another way would be the use of pre-synthesized (commercial) aqueous solution of AuNPs. However, it would be tedious to immobilize them onto the PDMS channel walls because of very high hydrophobicity of PDMS and poor affinity of particles to PDMS surface which would lead to a high probability of leaching (Buonerba et al., 2012). A preliminary treatment of PDMS surface with 3-aminopropyltriethoxysilane (γ–APTES) has been suggested to resolve this issue (Trung et al., 2012).

Kinetic data are scarce in the case of a microfluidic environment, when the small dimensions induce some distinct properties (Ben-Yoav et al., 2012). Studying the kinetics of a chemical reaction provides a mathematical tool for the clear understanding of the underlying mechanism.

Miniaturization of the reaction platforms provides new opportunities for advanced synthesis, and opens up many possibilities for a broad range of novel applications (Badilescu and Packirisamy, 2012; Demello, 2006). In micro-reactors, both heat and mass transport are considerably accelerated due to high surface area to volume ratios within the microchannels, allowing rapid and homogeneous mixing. A great variety of nanoparticles have been synthesized in a microfluidic environment and their quality in terms of size distribution has also been emphasized (Chan et al., 2003; Shalom et al., 2007; Song et al., 2005). The majority of these works were carried out by mixing liquid reactants in a microfluidic channel, using either a continuous flow, or droplet-based methods. In spite of the qualitative assessment of the high reaction rates in microchannels, few works focused specifically on the evaluation of the kinetic parameters (Batabyal et al., 2012; Roder et al., 2006; Song and Ismagilov, 2003). In the case of *in-situ* heterogeneous reaction, the reaction takes place either inside, or on the surface of a polymer network. One of the reactants is the polymer itself or a component of the polymer compound and therefore the reaction rate is low. To the best of our knowledge, the kinetics of an *in-situ* synthesis in a microfluidic environment has not been studied in detail.

In this work, a novel nano-integrated microfluidic biosensor is proposed for the detection of antigen–antibody (Ag–Ab) interaction through the LSPR properties of gold nanoparticles. For this purpose, the kinetics of the *in-situ* synthesis of Au–PDMS nanocomposite in a microfluidic chip is thoroughly investigated. The particularities of this reaction compared with the one carried out at macro-level are highlighted and the reduction mechanism of the gold ions in the microchannel is also discussed.

The sensitivity of the synthesized nanoparticles to the surrounding medium is then studied to assess the biosensing capability of the sensing platform. The microfluidic biosensor is further used for the detection of bST. The results show an enormous potential of the proposed biosensor in clinical applications.

2. Material and methods

2.1. Materials

A Sylgard® 184 elastomer kit from Dow Corning Corporation was used for PDMS fabrication and SU-8 (SU-8 2035) was purchased from MicroChem. Gold chloride trihydrate ($HAuCl_4 \cdot 3H_2O$) was purchased from Alfa Aesar and 1-pentanol, toluene, N,N-dimethylformamid, 2-propanol and ethyl alcohol from Sigma-Aldrich. Nanothink® 18, TWEEN® 20, N-hydroxysuccinimide (NHS), and N-(3-dimethylaminopropyl)-N′-ethylcarbodiimide hydrochloride (EDC) were purchased from Sigma-Aldrich. A monoclonal bovine growth hormone antibody (anti-BGH or bST) in mouse and BGH antigen were purchased from Dr. Parlow National Hormone and Peptide Program in California, USA.

2.2. Fabrication of microfluidic chip and in-situ synthesis of Au–PDMS nanocomposite

The PDMS microfluidic chip (or cell) was fabricated using a SU-8 (from MicroChem) mold. For the mold fabrication, the SU-8 was spin-coated to a thickness of 60 μm (at 500 rpm for 15 s followed by 2000 rpm for 30 s) on a cleaned 4″ wafer and then soft-baked at 95 °C for 10 min. The soft-backed SU-8 was exposed to UV light for 35 s (with exposure energy of 180 mJ/cm^2) followed by a post-baking process for 7 min at 95 °C. Afterward, the SU-8 was developed in SU-8 developer (from MicroChem). Finally the mold was hard-baked at 200 °C for 15 min. These steps are schematically illustrated in Fig. 1a (steps 1–4). The mold was finally silanized in vapor phase to enable removing of PDMS from the mold after curing. In the silanization process, a few drops of (tridecafluoro-1,1,2,2-tetrahydrooctyle)-1-trichlorosilane were introduced into a closed chamber with wafer while the chamber was kept at 65 °C on a hot plate for 3 h.

The PDMS compound was obtained by mixing PDMS with its curing agent (cross-linking agent) at a weight ratio of 10:1 and then degassed for a duration of 10 min. The mixture is then poured into the SU-8 mold and, after a second degasifying process the mold is kept in an oven at 60 °C overnight. Afterward, the cured molded PDMS is peeled off from the mold as shown in Fig. 1a (step 5). A flat PDMS layer (Fig. 1a-step 6) was then bonded using oxygen plasma treatment with the prepared channel layer to close the channel. For the plasma bonding, a Harrick Plasma Cleaner was used. In Fig. 1a, a chip with two channels of 400 μm width is shown. For simplicity, it will be referred as C400-2 (400-2 microfluidic chip), where the first and second terms indicate the width of channel and the number of channels, respectively. In this work two microfluidic chips (C400-1 and C400-2) were used for the experiments. The depth of the microchannel(s) in all chips is 60 μm.

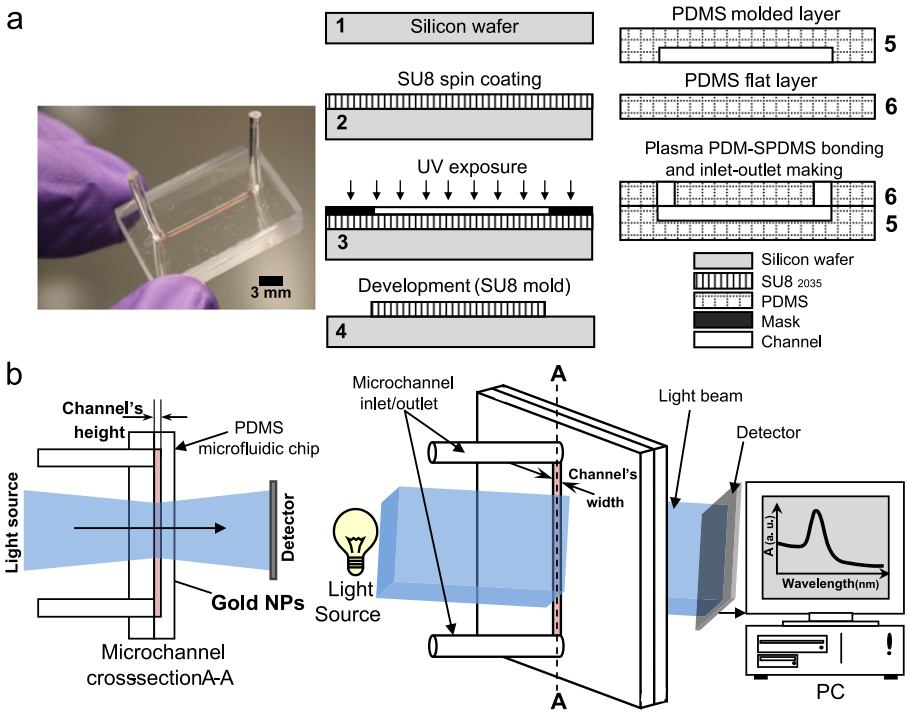

Fig. 1. Fabrication procedure of microfluidic chip and measurement of the spectral band; (a) step-by-step fabrication procedure of SU-8 mold and PDMS microfluidics; the figure shows a chip with two channels (C400-2) and the red color of the channels indicates the synthesized AuNPs; and (b) the microfluidic chip was placed directly in a spectrophotometer in order to measure the gold plasmon band. (For interpretation of the references to color in this figure legend, the reader is referred to the web version of this article.)

Aqueous solutions of chloroauric acid with different concentrations were prepared. For the fabrication of gold–PDMS nanocomposite in a macro-environment, the flat PDMS samples were cut into 1 cm × 4 cm pieces and the samples were incubated in the gold precursor solution for different durations (SadAbadi et al., 2012). In order to prepare gold nanocomposite inside the microfluidic chip through the *in-situ* synthesis, the gold solution was introduced into the microchannel with a syringe (~5 μl) and then the whole chip was kept at different temperatures for different durations. In order to avoid the evaporation of the solution, the inlet/outlet was closed. In Fig. 1a, fabricated microchannels with gold nanocomposite (red channels) is shown. The synthesis time for this cell was 48 h.

As shown in our previous work (SadAbadi et al., 2012), the curing agent in PDMS reduces the gold ions to gold nanoparticles embedded into the polymer network. Relatively high concentrations of gold precursor were used in order to increase the rate of the reaction. The effects of the concentration of gold precursor (ranging from 0.5% to 2%) and of the temperature (22 °C, 40 °C, and 50 °C) on the kinetics of the synthesis reaction were investigated. The gold nanocomposites formed in the microchannel have been characterized using UV–visible spectroscopy and scanning electron microscopy (SEM).

The gold plasmon bands of the microfluidic chips were measured using a UV/vis spectrophotometer (LAMBDA 650 UV/vis Spectrophotometer from PerkinElmer) as schematically shown in Fig. 1b (Haes and Van Duyne, 2004). In some cases, the magnitude of the absorbance was low due to low amount of Au nanoparticles in the channel, resulting in a noisy spectrum. A denoising MATLAB® code based on wavelet analysis was used to remove the low frequency noises (SadAbadi et al., 2007) in these cases.

In order to obtain the size distribution of particles from SEM images, Gwyddion 2.28, a modular program for data visualization and analysis was used. Several SEM images with similar magnification were used to obtain the size distribution histogram.

In addition, the samples were annealed to improve the distribution of gold NPs embedded in PDMS. Heat treatment (annealing) was found to increase the concentration of AuNPs on the surface of the sample. For annealing, the samples have been heated from room temperature to 300 °C in 10 min and then kept at this temperature for 30 min. It was observed that temperature higher than 350 °C is not suitable as it results in deformation of the chip.

2.3. Sensitivity tests

Generally, the Au-LSPR band is known to shift to longer wavelengths (red-shift) as the surrounding medium's refractive index (n) is increased (Wang et al., 2006). The sensitivity of the Au-nanocomposite microfluidic platform with respect to the environments with different refractive indices has been investigated. For this purpose, five solvents with different refractive indices have been selected. Each solvent was passed through a C400-2 and the corresponding LSPR band was recorded. The sensitivity for each chip (both annealed and non-annealed samples) has been calculated from the variation of $\Delta\lambda_{max}$ against Δn, where $\Delta\lambda_{max}$ in nanometer is the difference in the position of peak wavelength corresponding to the Au-LSPR band using solvent and deionized water, and Δn is the refractive index difference between the solvent and DI-water and is given by $\Delta n = n_{solvent} - n_{water}$ where $n_{water} = 1.33$.

2.4. Biosensing protocol

Label-free biosensing tests have been performed by using the annealed C400-2. The bST antibody (anti-BGH) obtained in mouse and its corresponding antigen (Ag) were used for biosensing experiments.

The first step of biosensing protocol consists of functionalizing the gold nanoparticles with 11-mercaptoundecanoic acid (NanoThink® ACID11) in ethanol (5 mM), by introducing the solution into the microchannel and keeping it for at least 5 h. After attaching the linker, the conventional carbodimide coupling chemistry (EDC/NHS) is used to activate the carboxyl groups, before attaching the antibody (Ab).

The activation is carried out by injecting a mixture of N-(3-dimethylaminopropyl)-N′-ethylcarbodiimide hydrochloride (EDC, 0.4 M) and N-hydroxysuccinimide (NHS, 0.1 M) for 1 h (1:1 ratio by volume). The next step consists of attaching the antibody dissolved in a PBS buffer solution (200 ng/ml) to the functionalized AuNPs, followed by washing the microchannel several times with a TWEEN® 20 solution in PBS (0.05%). The last step is attaching the Ag dissolved in a buffer solution by injecting the growth hormone solution into the microchannel. The growth hormone solution was obtained by mixing different concentrations of bST in buffer solution. The samples were washed carefully with PBS afterward. The LSPR spectra of the microfluidic cell were recorded after each step. Different antigen concentrations were tested in order to obtain the limit of detection for the proposed biosensor.

3. Results and discussion

3.1. In-situ synthesis and study of reaction kinetics

The following reduction reaction between the gold ions and curing (cross-linking) agent has been suggested (Zhang et al., 2008):

$$3\,\mathrm{Si}-\mathrm{H}+(3/2)H_2O+2AuCl_4^- \rightarrow (3/2)-\mathrm{Si}-O-\mathrm{Si}-2Au+8Cl^-+6H^+$$

In order to characterize the Au–PDMS nanocomposite formed inside the microchannel, UV/vis spectroscopy was used. The formation of gold–PDMS nanocomposite has been studied by using chips with different configurations. Based on the results, the absorbance was found to vary linearly with the number of channels and the width of the channel. For instance, for similar synthesis conditions (time, temperature, and gold salt concentration), the absorbance of a cell with three channels is about three times higher than that of a cell with only one channel of similar widths. However, due to small values of absorbance for microfluidic cells, a higher absorbance generally has the advantages of less noise in the spectra and an improved accuracy.

To study the kinetics of gold synthesis in a microfluidic environment, the UV–visible spectra of a microfluidic chip (C400-1) under different concentrations (1% and 2% of gold salt) and temperatures (22 °C, 40 °C and 50 °C) were measured (Fig. 2a and c).

Fig. 2a shows that the kinetics of formation of AuNPs is similar for 1% and 2% gold salt concentrations. However, the absorbance is higher for higher concentration of the gold salt, due to higher number of particles formed in a unit area. The graph shows that the evolution of the reduction reaction can be described through three main phases: induction, when there are only a few particles on the surface; the actual formation step, when the absorbance shows a linear relationship with time and, and finally, the step of saturation. As shown in Fig. 2a, the induction step takes around 3–5 h and the saturation phase was reached only after around 5 days (130 h) of reaction.

The long induction and reaction times can be related to the particularities of the *in-situ* reaction. The reaction takes place between the gold ions in an aqueous solution and the cross-linking agent (a vinyl silicon compound) that is embedded in the polymer network. The amount of the cross-linking agent (curing agent) available for the reduction of Au^{3+} depends on the ratio of pre-polymer to cross-linking agent used for the fabrication of PDMS. The reductant molecules migrate toward the surface of the channel and their diffusion is very slow (dashed arrows in Fig. 2f). The effect of the concentration of the cross-linking agent on the *reaction rate constant* (k^*) is shown in Fig. 2b. It can be seen that the rate constant increased considerably when the PDMS was fabricated by using a higher amount of cross-linking agent (4:1 compared with 10:1). This experiment confirms the claim that the cross-linking agent acts as a reductant.

In addition, the effect of temperature was investigated to have a more clear understanding of the kinetics of the reduction of gold ions in micro-environment. Fig. 2c shows the first 30 h of evolution of the reaction in a C400-1, corresponding to three different temperatures (22 °C, 40 °C, and 50 °C). The absorbance–time slope (linear segment of Fig. 2c) was used to calculate the apparent reaction rate constants. The apparent rate constants (k^*) of the reduction reaction are shown in Table 1 for different temperatures. In this table, the induction time (in minutes) and the half-life of the reaction, $\tau_{1/2}$, are also given. The data were derived here from spectrometric measurements, and therefore, they are denoted as apparent rates and apparent activation energy.

The Arrhenius equation is used to calculate the activation energy E_a of a reaction as follows:

$$k = Ae^{-E_a/RT} \rightarrow \ln(k) = -\frac{E_a}{R}\frac{1}{T} + \ln(A) \quad (1)$$

where A is the pre-exponential (or frequency) factor, k is the rate constant of the reaction at the temperature T (in Kelvin) and R is the universal gas constant (R=8.314 J/mol K). The activation energy is expressed in J/mol.

Considering that the gold ion reduction reaction has a rate constant that obeys the Arrhenius equation, a plot of $\ln(k^*)$ (in s^{-1}) versus T^{-1} follows a straight line as shown in Fig. 2d. The slope of the Arrhenius plot (Fig. 2d) was used to extract the apparent activation energy, E_a^*, of the reaction using the following equation:

$$E_a^* = -R\left(\frac{\ln(k)}{1/T}\right) = 29.8 \ \text{kJ/mol} \quad (2)$$

The relatively large value of the activation energy ($E_a^* \approx 30$ kJ/mol) shows that the reaction needs a high energy contribution. The reaction is facilitated at high temperatures when the migration of the reducing agent is faster.

The apparent rate constant, determined in the microchannel environment is compared with the reaction carried out at the macro-scale (SadAbadi et al., 2012) under similar conditions and the results are compared in Fig. 2e. The reaction rate in microfluidic environment is $k^* = 4.6 \times 10^{-4}\ \mathrm{h}^{-1}$ and in macro-environment is $k^* = 7.3 \times 10^{-3}\ \mathrm{h}^{-1}$. These results show that the reaction is approximately 16 times slower in the microchannel due to less favorable conditions for mixing of the reactants. The schematic shown in Fig. 2f illustrates how the reduction reaction takes place in the microchannel. It also shows how the migration of the cross-linking agent to the channel surface can take place. The lower reaction rate in the microfluidic environment is also due to the effect of the channel wall that may adsorb (immobilize) the gold ions and the cross-linking agent. Therefore, in the case of this *in-situ* heterogeneous reaction, the microfluidic environment has not enhanced the rate of reaction for the tested conditions. However, as seen in Section 3.2, the size distribution of gold NPs synthesized in the microchannel was significantly narrower providing better uniformity in the size of the particles

3.2. Particle size distribution in micro- and macro-environments

SEM imaging was used to characterize the size distribution of AuNPs in the annealed microchannel. In order to take the image of the particles inside the channels, the PDMS–PDMS bonding was removed. Fig. 3a shows the SEM image of particles formed in a C400-1 microfluidic cell prepared by introducing a 1% solution of gold precursor for 24 h in the channel. The channel edge is seen in the SEM image. The inset of the figure shows a close-up of gold particles with a size of around 120 nm.

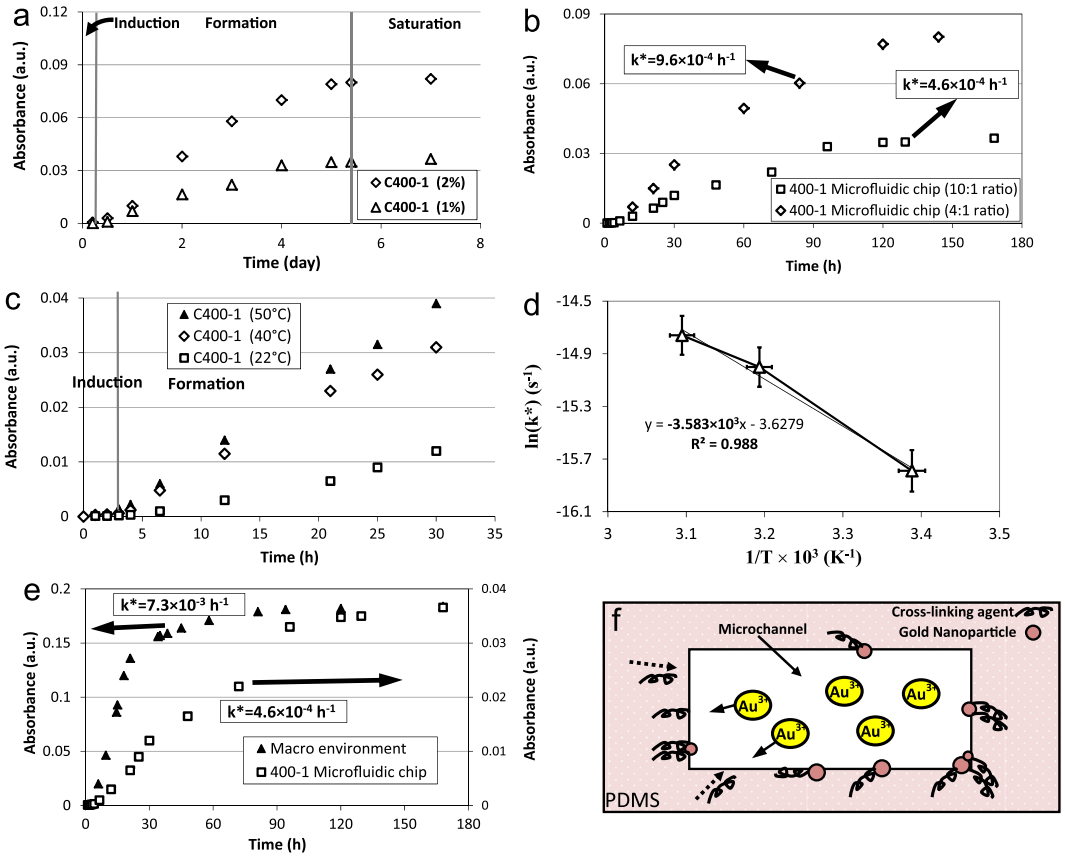

Fig. 2. Study of the kinetics of the reduction reaction; (a) absorbance–time plots of the reaction in C400-1, corresponding to 1% and 2% gold salt concentrations at room temperature, (b) the effect of PDMS cross-linking agent on the evolution of gold nanoparticles formation, (c) the effect of temperature on the formation of gold nanoparticles by using 1% gold salt solution, (d) the Arrhenius plot for the calculation of apparent activation energy, (e) comparison of the formation of gold in a PDMS microchannel and in a macro-scale environment, and (f) illustration of the *in-situ* reaction in the channel cross-section and the migration of reducing agent (dashed arrows) toward the channel wall.

Table 1
Apparent rate constants of the formation of gold NPs at different temperatures.

Temperature (°C)	Induction time (min)	$\tau_{1/2}$ (min)	k^* (h^{-1})
22 ± 0.5	330	3960	0.5×10^{-3}
40 ± 0.5	240	3540	1.1×10^{-3}
50 ± 0.5	180	3360	1.4×10^{-3}

The annealing process improves the uniformity of the particle morphology as can be seen in the SEM images by a narrower size distribution and less particle aggregations, indicated by the blue-shift of the Au-LSPR band (SadAbadi et al., 2012). The improvement is evaluated by a blue-shift of the band which is ~8 nm shift in macro-environment compared with only ~2 nm shift in a microchannel environment after annealing. This is due to the fact that the distribution of the synthesized particles in the non-annealed micro-channel is more uniform than in the sample prepared in macro-environment, even before annealing. Therefore it can be inferred that the annealing treatment does not have a significant effect of the gold nanoparticles prepared in a microfluidic environment.

In order to show the difference between the size distributions of gold nanoparticles prepared in the microfluidic chips and the particles prepared in a macro-environment, gold nanocomposites were prepared in microchannel as well as in a macro-environment. Gold nanoparticles integrated microfluidic chip was prepared by keeping a 2% solution of gold salt for 48 h in the channel. The same conditions are used to fabricate a gold–PDMS nanocomposite by incubating PDMS samples in gold solution (macro-environment). Both samples were annealed. SEM images and the corresponding histograms of particle size distribution for the C400-1 and for macro-sample are shown in Fig. 3b and c, respectively. Fig. 3b illustrates that the distribution of the particles in the microchannel is narrower than in the macro-environment (Fig. 3c) which is one of the advantages of microfluidic synthesis. It could be seen in Fig. 3b and c that the particle size in the channel has a band of 125 ± 5 nm compared to the bandwidth of 140 ± 35 nm in macro-sample. This is in agreement with the shape of the gold-LSPR band in both micro- and macro-sample as shown in Fig. 3d.

It should be noted that the *in-situ* reaction has been performed in a static way, meaning that the reactant (gold solution) was not flown continuously through the channel during the synthesis. In spite of this, the size distribution of the AuNPs was found to be narrower compared with the batch method (macro-environment). In the batch method, growing of the gold crystals cannot be controlled while in the microfluidic channel the growing is confined to the free volume in the polymer network. There is a physical limit to which the gold crystals can grow in the polymer network inside the channel due to the confinement and this leads to higher uniformity in spite of using the static procedure.

Narrower particle distribution on the surface will result in improved sensitivity of the microfluidic platform and could improve the detection limit of the proposed biosensor. Narrower size distribution indicates the availability of more AuNPs of similar size. It indicates that each gold nanoparticle will be surrounded by approximately the same number of biomolecules during the binding of antibodies, forming a uniform layer. This will lead to a narrower ;Au-LSPR band in the final step of

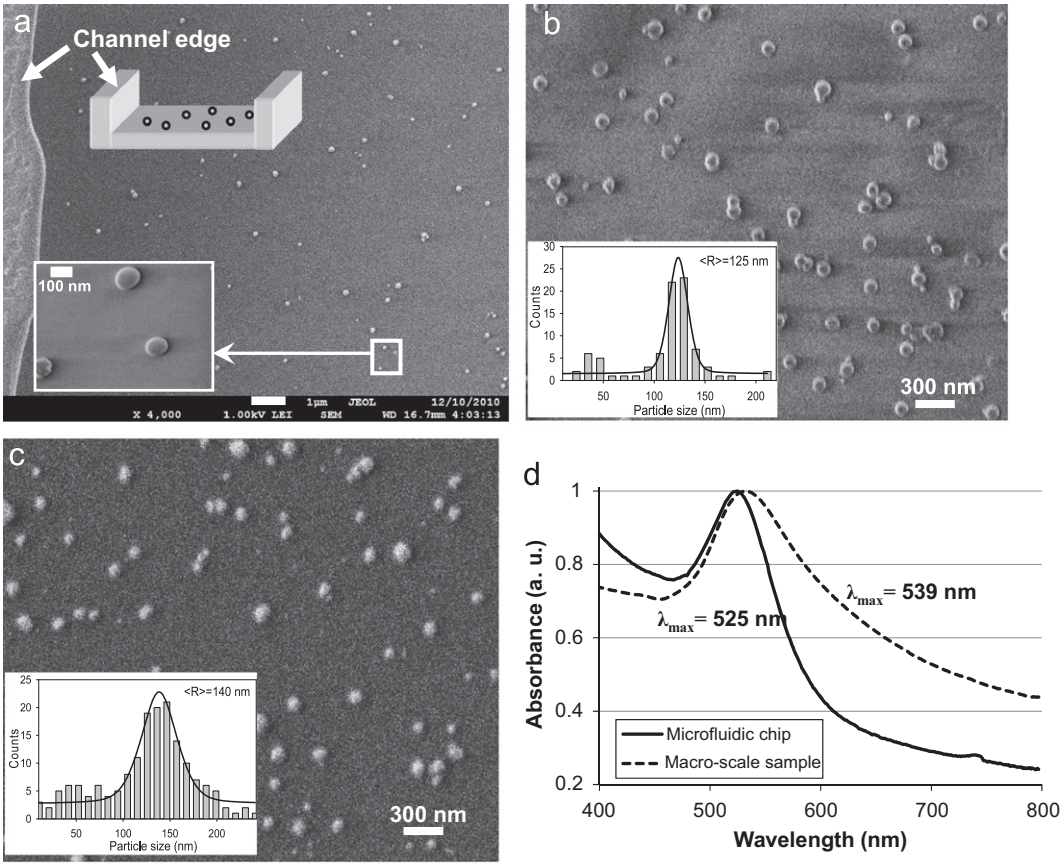

Fig. 3. SEM images and particle size distribution of annealed cells; (a) a microchannel and formation of gold NPs on the channel surfaces; at the left side, the channel edge is shown and the inset shows the shape of particles. (b,c) SEM image and the corresponding size distribution of gold NPs prepared by 2% solution of gold precursor for 48 h of incubation for two different (c: microchannel and d: macro-scale) environments and (d) Au-LSPR band of nanocomposites prepared in microchannel and macro-scale environment.

biosensing and hence the wavelength shift can be found with high precision.

3.3. Sensing experiments

3.3.1. Sensitivity test

The sensitivity test is a good way to assess the biosensing capability of a sensing platform. In order to determine the sensitivity of the platform, experiments were conducted in media of different refractive indices (RI). By increasing the refractive index of the surrounding medium, the Au-band is shifted to longer wavelengths. For this purpose, two sets of five identical 400-2 chips were prepared and one set was annealed. Each solvent was introduced into the channel and its spectrum was recorded. The sensitivity graphs for both non-annealed and annealed cells are shown in Fig. 4.

The results show that the annealed sample has a sensitivity as high as 74 nm/RIU which makes it very useful for label-free biosensing application. The sensitivity for the non-annealed samples is about 65 nm/RIU. The similar values of sensitivity show that the annealing treatment has less effect on the uniformity in a microfluidic environment as discussed earlier in Section 3.2.

3.3.2. Biosensing capability of the proposed biosensor and the limit of detection of BGH

The microfluidic biosensor integrated with gold NP, prepared and annealed as described earlier, was tested for the biosensing of bST. The biosensing experiment involves the detection of antigen–antibody interaction of bovine growth hormone through the measurement of LSPR spectra of the samples recorded at different steps. Annealed C400-2 microfluidic cells were used for these tests. A cross-section of the microchannel with embedded gold nanoparticles is schematically shown in Fig. 5a and different steps of the biosensing experiment are depicted in Fig. 5b.

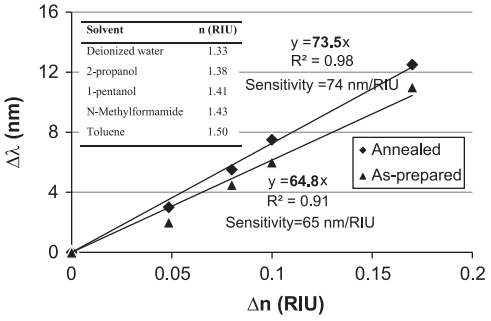

Fig. 4. Sensitivity tests of the 400-2 microfluidic cell prepared from 2% aqueous solution of gold for 48 h.

During the biosensing experiment, biomolecules immobilize to the AuNPs and this attachment results in the increased refractive index of the surrounding medium of gold nanoparticles. Consequently the Au-LSPR band shifts to longer wavelengths after each step. During the last step (attaching of the Ag) the shift is mainly due to the Ab–Ag interaction. The spectra corresponding to the different steps of the biosensing experiment are shown in Fig. 5d. In order to obtain the detection limit of the proposed biosensor for the detection of growth hormone, antigen with different concentrations (80 ng/ml, 40 ng/ml,

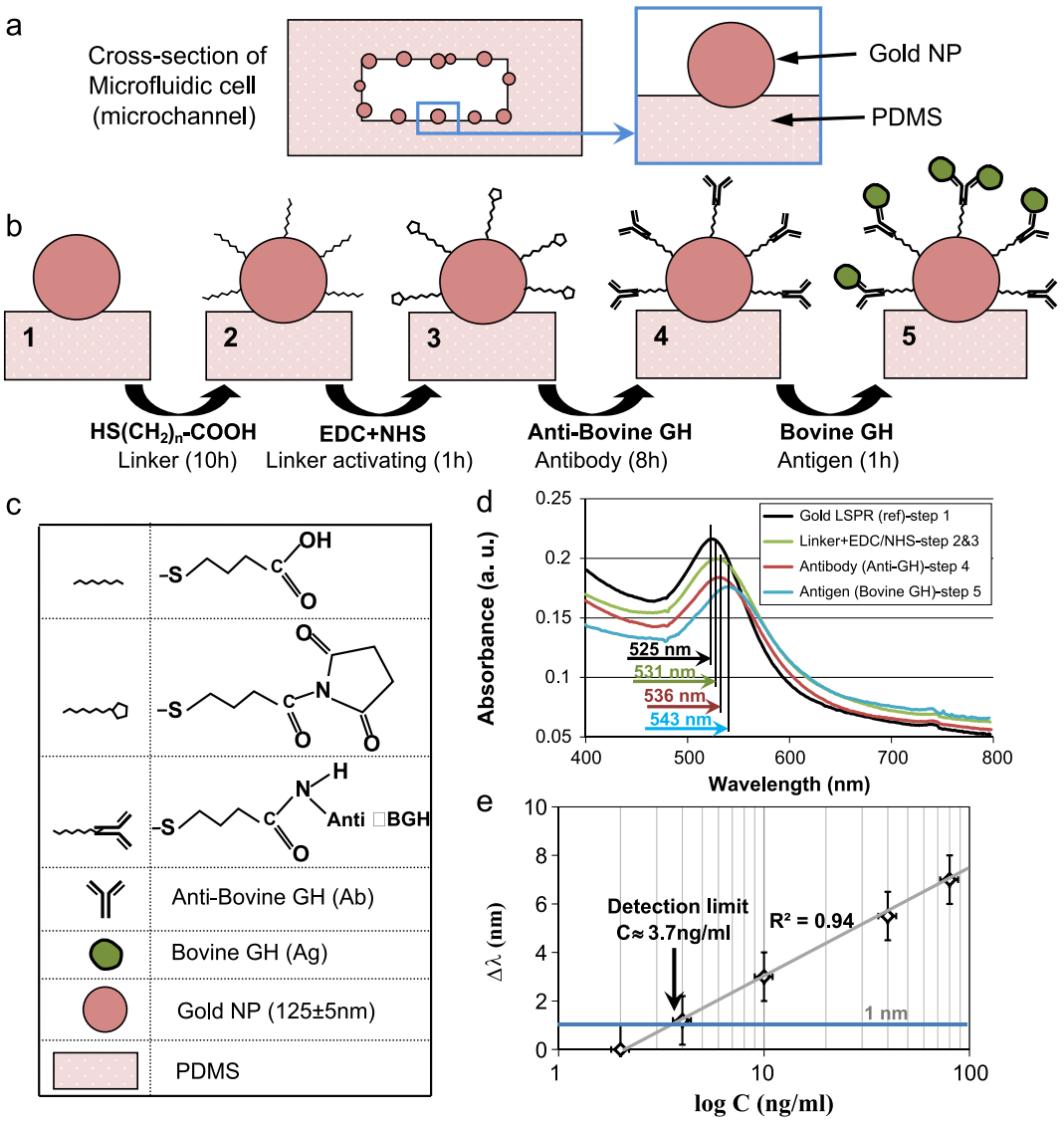

Fig. 5. Biosensing experiments performed by using the annealed microfluidic biosensor (400-2 cells) prepared from 2% aqueous solution of the gold precursor (48 h): (a) cross-section of a microchannel and AuNPs in the channel; (b) four steps of the biosensing protocol; (c) legend of the schematics; (d) Au-LSPR corresponding to the four sensing steps depicted in (a); and (e) LSPR band shift corresponding to different Ag concentrations.

10 ng/ml, 4 ng/ml, and 2 ng/ml) were tested for biosensing. These concentrations were imposed by the actual concentration of the bST in the milk. As mentioned earlier, it has been reported that the concentration of bovine somatotropin (bST) in milk could be less than 10 ng/ml (McGrath et al., 2008). A broader range of concentration was considered in order to establish the operation range of the sensor.

The Au-LSRP shift corresponding to the last biosensing steps (steps 4 and 5) was recorded for each concentration. A detection limit of 3.7 ng/ml (185 pM) is estimated by interpolation as shown in Fig. 5e considering 1 nm precision of the measurement. The measured variation of red-shift against the concentration of bovine growth hormone in Fig. 5e proves the applicability of the proposed sensor for the detection of a wide range of bST concentration.

4. Conclusions

Gold–PDMS nanocomposite was synthesized in a microfluidic channel through an *in-situ* reaction between a gold precursor and the cross-linking (curing) agent of the polymer. It was found that the reaction is slower in microfluidic environment than in a macro-scale. However, the size distribution of gold nanoparticles synthesized in the microchannel was found to be 120–130 nm (8% size variation) while the size distribution in the macro-scale was in 105–175 nm range (67% size variation). Hence, it was concluded that the *in-situ* microfluidic synthesis resulted in an order of magnitude (8.3 times) improvement in size uniformity. The kinetics of the *in-situ* synthesis in microfluidic environment was studied in detail and the apparent activation energy of the reaction was estimated to be $E_a^* \approx 30$ kJ/mol using the Arrhenius equation.

The capability of the proposed microfluidic biosensor to detect growth hormone based on antibody–antigen interaction was successfully demonstrated. The detection limit was found to be as low as 3.7 ng/ml (185 pM). This strategy demonstrated a successful integration of microfluidics and nanoparticles that can potentially provide an alternative method for the clinical detection of polypeptides and proteins.

It should be noted that some components should be miniaturized in order to have a portable device for possible commercialization of the proposed biosensor. It is suggested to use an on-chip optical detector or to use miniaturized spectrophotometers for the LSPR

detection of the analyte. Indeed, the microfluidic device should be integrated with flow cells and possibly a micropump in order to be able to rinse the microfluidic channel and restore the sensor for the next measurement.

References

Abbas, A., Linman, M.J., Cheng, Q., 2011. Biosensors and Bioelectronics 26, 1815–1824.
Arlett, J., Myers, E., Roukes, M., 2011. Nature Nanotechnology 6, 203–215.
Badilescu, S., Packirisamy, M., 2012. Polymers 4, 1278–1310.
Barnes, W.L., Dereux, A., Ebbesen, T.W., 2003. Nature 424, 824–830.
Batabyal, S., Rakshit, S., Kar, S., Pal, S.K., 2012. Review of Scientific Instruments 83, 43113.
Ben-Yoav, H., Dykstra, P.H., Bentley, W.E., Ghodssi, R., 2012. Biosensors and Bioelectronics 38, 114–120.
Buonerba, A., Cuomo, C., Ortega Sánchez, S., Canton, P., Grassi, A., 2012. Chemistry—A European Journal 18, 709–715.
Chan, E.M., Mathies, R.A., Alivisatos, A.P., 2003. Nano Letters 3, 199–201.
Cheng, X., Chen, G., Rodriguez, W.R., 2009. Analytical and Bioanalytical Chemistry 393, 487–501.
Demello, A.J., 2006. Nature 442, 394–402.
Geng, Z., Liu, W., Wang, X., Yang, F., 2011. Sensors and Actuators A: Physical 169, 37–42.
Haes, A.J., Van Duyne, R.P., 2002. Journal of American Chemical Society 124, 10596–10604.
Haes, A.J., Van Duyne, R.P., 2004. Analytical and Bioanalytical Chemistry 379, 920–930.
Hoa, X., Kirk, A., Tabrizian, M., 2009. Biosensors and Bioelectronics 24, 3043–3048.
Hsu, W.T., Hsieh, W.H., Cheng, S.F., Jen, C.P., Wu, C.C., Lee, C.Y., Li, W.Y., Chau, L.K., Chiang, C.Y., Lyu, S.R., 2011. Analytica Chimica Acta, 75–82.
Huang, C., Bonroy, K., Reekman, G., Verstreken, K., Lagae, L., Borghs, G., 2009a. Microelectronic Engineering 86, 2437–2441.
Huang, C., Bonroy, K., Reekmans, G., Laureyn, W., Verhaegen, K., De Vlaminck, I., Lagae, L., Borghs, G., 2009b. Biomedical Microdevices 11, 893–901.
Kim, J., Hong, J.W., Kim, D.P., Shin, J.H., Park, I., 2012. Lab on a chip 12, 2914–2921.
Le Breton, M.H., Beck-Henzelin, A., Richoz-Payot, J., Rochereau-Roulet, S., Pinel, G., Delatour, T., Le Bizec, B., 2010. Analytica Chimica Acta 672, 45–49.
Li, Y.T., Liu, H.S., Lin, H.P., Chen, S.H., 2005. Electrophoresis 26, 4743–4750.
Lin, C.C., Wang, J.H., Wu, H.W., Lee, G.B., 2010. Journal of the Association for Laboratory Automation 15, 253–274.
Luo, Y., Yu, F., Zare, R.N., 2008. Lab on a Chip 8, 694–700.
McGrath, M.F., Bogosian, G., Fabellar, A.C., Staub, R.L., Vicini, J.L., Widger, L.A., 2008. Journal of Agricultural and Food Chemistry 56, 7044–7048.
Ozhikandathil, J., Badilescu, S., Packirisamy, M., 2012. IEEE Sensors Journal 12, 2791–2798.
Ozhikandathil, J., Packirisamy, M., 2012. Biomicrofluidics 6, 046501.
Qiu, J.D., Wang, L., Liang, R.P., Wang, J.W., 2009. Electrophoresis 30, 3472–3479.
Roder, H., Maki, K., Cheng, H., 2006. Chemical Reviews 106, 1836–1861.
SadAbadi, H., Badilescu, S., Packirisamy, M., Wuthrich, R., 2012. Journal of Biomedical Nanotechnology 8, 539–549.
SadAbadi, H., Ghasemi, M., Ghaffari, A., 2007. Biomedical Papers of the Medical Faculty of the University Palacky Olomouc Czech Republic 151, 73–78.
Shalom, D., Wootton, R.C.R., Winkle, R.F., Cottam, B.F., Vilar, R., demello, A.J., Wilde, C.P., 2007. Materials Letters 61, 1146–1150.
Song, H., Ismagilov, R.F., 2003. Journal of the American Chemical Society 125, 14613–14619.
Song, Y., Doomes, E., Prindle, J., Tittsworth, R., Hormes, J., Challa, S., Kumar, R., 2005. Journal of Physica Chemistry B 109, 9330–9338.
Trung, N.B., Yoshikawa, H., Tamiya, E., Viet, P.H., Takamura, Y., Ashahi, T., 2012. Japanese Journal of Applied Physics 51, 037001.
Wang, H., Wu, Y., Lassiter, B., Nehl, C.L., Hafner, J.H., Nordlander, P., Halas, N.J., 2006. Proceedings of the National Academy of Sciences of the United States of America 103, 10856–10860.
Zhang, Q., Xu, J.J., Liu, Y., Chen, H.Y., 2008. Lab on a Chip 8, 352–357.
Zhang, T., He, Y., Wei, J., Que, L., 2012. Biosensors and Bioelectronics 38, 382–388.
Zhou, F., Lu, M., Wang, W., Bian, Z.P., Zhang, J.R., Zhu, J.J., 2010. Clinical Chemistry 56, 1701–1707.